

www.acsami.org Research Article

# Enhancing the Solubility of Semiconducting Polymers in Eco-Friendly Solvents with Carbohydrate-Containing Side Chains

Madison Mooney, Yunfei Wang, Audithya Nyayachavadi, Song Zhang, Xiaodan Gu,\* and Simon Rondeau-Gagné\*



Cite This: https://doi.org/10.1021/acsami.1c02860



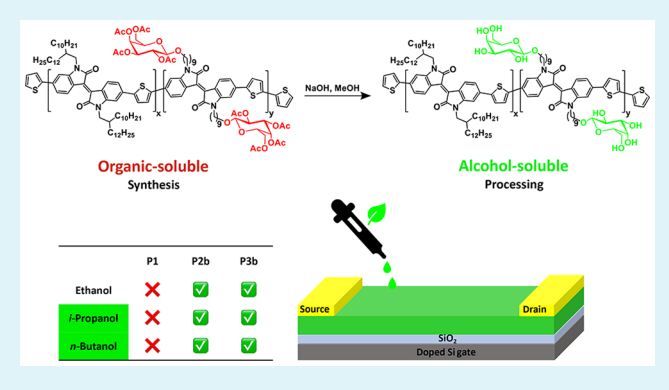
**ACCESS** I

III Metrics & More

Article Recommendations

SI Supporting Information

ABSTRACT: Semiconducting polymers are at the forefront of next-generation organic electronics due to their robust mechanical and optoelectronic properties. However, their extended  $\pi$ -conjugation often leads to materials with low solubilities in common organic solvents, thus requiring processing in high-boiling-point and toxic halogenated solvents to generate thin-film devices. To address this environmental concern, a natural product-inspired side-chain engineering approach was used to incorporate galactose-containing moieties into semiconducting polymers toward improved processability in greener solvents. Novel isoindigo-based polymers with different ratios of galactose-containing side chains were synthesized to improve the solubilities of the organic semiconductors in alcohol-based solvents. The



addition of carbohydrate-containing side chains to  $\pi$ -conjugated polymers was found to considerably impact the intermolecular aggregation of the materials and their microstructures in the solid state as confirmed by atomic force microscopy and grazing-incidence wide-angle X-ray scattering. The charge transport characteristics of the new semiconductors were evaluated by the fabrication of organic field-effect transistors prepared from both toxic halogenated and greener alcohol-based solvents. Importantly, the incorporation of carbohydrate-containing side chains was shown to have very little detrimental impact on the electronic properties of the polymer when processed from green solvents.

KEYWORDS: green electronics, semiconducting polymers, organic field-effect transistors, side-chain engineering, processing of  $\pi$ -conjugated polymers

# INTRODUCTION

Today, with rapidly evolving connections between humans and their surroundings, the so-called Internet of Things (IoT), data is continuously being acquired, received, and transmitted wirelessly by many types of households, consumers, and industrial objects. 1-3 To take the next steps to advance the IoT, next-generation electronics have to be capable of being processed in different shapes and forms.<sup>4</sup> More importantly, these electronics need to expand their versatility to be used directly on (or inside) the human body to enhance our connectivity to the environment and, ultimately, develop new applications such as personalized health care and large-scale energy production. 5-8 With the potential to be cheaper than current electronics and the capability to be stretchable and conformable, organic-based semiconductors have an enormous potential for use in the fabrication of next-generation electronics. In a short time, major progress has been made in this field, including the synthesis of high-performance semiconducting polymers, preparation of materials with selfhealing properties, and synthesis of intrinsically stretchable conductors. flo-12 However, with the ever-increasing pace of technological advancements and the fact that outdated electronic disposal releases metals and other toxic elements into the land and sea, causing toxic environmental hazards, the cost of these new electronics to the environment needs to be considered.

Semiconducting polymers have been shown to be particularly efficient in the fabrication of flexible and stretchable electronics.  $^{13-15}$   $\pi$ -Conjugated polymers have good charge transport and electronic properties, their synthesis and preparation are well-known, and they can generate active materials at a lower cost than traditional silicon-based materials. Additionally, their mechanical properties (especially their elastic moduli) and optical properties are also advantageous for the design of new electronics, which makes these

Received: February 10, 2021 Accepted: May 5, 2021



Scheme 1. Synthetic Pathway for the Preparation of Semiconducting Polymers P1b to P4b

materials particularly promising for developing bioinspired devices. <sup>15–19</sup> Despite these important advantages, conjugated polymers suffer from an important limitation; these materials are mostly soluble in high-boiling-point, toxic halogenated organic solvents at elevated temperature, which undoubtedly limit their processability and implementation for the large-scale fabrication of emerging electronic devices.

In recent years, many important milestones have been achieved toward making  $\pi$ -conjugated polymers greener, especially by the development of novel pathways for their synthesis via direct heteroarylation polymerization (DHAP).<sup>20-22</sup> However, the tuning of their solubility is still a constant challenge. Several investigations of the processing of  $\pi$ -conjugated polymers in greener aromatic solvents, such as oanisole, in combination with the utilization of small-molecule additives have been reported. 23,24 New chemical designs and strategies have also been developed to improve solubility in alcohols and water. These include side-chain engineering with ionic moieties, <sup>25,26</sup> nonionic moieties, <sup>27,28</sup> and the incorporation of nonconjugated moieties (conjugation breaking units) that reduces the crystallinity of the polymer.<sup>29</sup> Among these reports, Woo et al. have recently reported the synthesis of a novel nonionic conjugated polymer incorporating branched oligoethylene glycol (OEG) side chains.<sup>30</sup> This polymer was shown to be highly soluble in ethanol and was directly utilized for the fabrication of OFET and OPV devices using ethanol as a processing solvent. Interestingly, the authors also showed that the utilization of ethanol significantly impacted the solidstate morphology, leading to an enhanced aggregation and edge-on orientation. Furthermore, You et al. used linear OEG side chains to achieve solubility of benzodithiophene and benzotriazole-based copolymers in 2-methyltetrahydrofuran

(2-MeTHF), a greener and renewable alternative solvent.31 They determined that solubility in greener solvents such as 2-MeTHF could be tuned by altering the percentage of OEG side chains in the polymers. Park et al. observed similar results with linear OEG side-chain functionalization of benzothiadia-zole-based polymers.<sup>32</sup> This approach led to solubility in nonhalogenated solvents such as 2-methyl anisole and 3methylcyclohexanone. Despite the development of these innovative strategies to modulate and control the solubility of semiconducting polymers in eco-friendly solvents, there are still challenges to be addressed before the large-scale fabrication of high-performance organic electronics in alcohol-based solvents and water can be realized, mostly due to the inverse relationship between crystallinity (charge transport) and solubility.

Herein, we report the side-chain modification of semicrystalline semiconducting  $\pi$ -conjugated polymers based on bioinspired (E)-1H,1'H-[3,3']biindolylidene-2,2'-dione (isoindigo) with carbohydrate-containing moieties.<sup>33</sup> The utilization of a side-chain engineering approach with galactose toward semiconducting polymers with tunable solubility in eco-friendly solvents was chosen for several reasons. First, carbohydrates are highly polar with multiple intermolecular hydrogen bonding sites, which can improve solubility in polar alcohol-based solvents and water, known to be particularly used in solution printing. Second, glycosylation and glucuronidation are effective and well-known strategies commonly used in medicinal and pharmaceutical chemistry to help the transition of lipophobic drugs and compounds in biological media, thus improving their delivery and enhancing their potency. 36-38 Given the current in-depth knowledge on such strategies, the attachment of protected galactose onto a

Table 1. Molecular Weights, Polydispersities, Optical Properties, and Energy Levels of Isoindigo-Based Polymers P1a to P4a and P1b to P4b

$$\begin{array}{c} \text{P1, } x = 0 \text{ mol}\% \\ \text{P2b, } x = 20 \text{ mol}\% \\ \text{P3b, } x = 50 \text{ mol}\% \\ \text{P4b, } x = 80 \text{ mol}\% \\ \text{P4b, } x = 80 \text{ mol}\% \\ \end{array}$$

polymer	$M_{\rm n}~({\rm kDa})^a$	$M_{\rm w} ({\rm kDa})^a$	$\overline{D}^{b}$	$\lambda_{\max \text{ (film)}} (nm)^c$	$E_{\rm g}^{\rm opt} ({\rm eV})^d$	HOMO (eV) <sup>e</sup>	LUMO (eV) <sup>f</sup>	$T_{\rm d}$ (°C) <sup>g</sup>
P1	20.6	28.0	1.4	698	1.52	-5.27	-3.75	389
P2a	14.8	28.8	1.9	700	1.52	-5.44	-3.92	380
P2b	14.0			701	1.50	-5.39	-3.89	384
P3a	11.1	22.3	2.0	699	1.53	-5.50	-3.97	360
P3b	11.1	22.3	2.0	707	1.50	-5.33	-3.83	355
P4a	8.7	11.2	1.3	706	1.51	-5.49	-3.98	358
P4b				717	1.43	-5.42	-3.99	302

"Number-average molecular weight and weight-average molecular weight estimated by high-temperature gel permeation chromatography in 1,2,4trichlorobenzene at 180 °C using polystyrene as the standard. <sup>b</sup>Dispersity defined as  $M_{\rm w}/M_{\rm n}$ . <sup>c</sup>Absorption maxima in the thin film. <sup>d</sup>Calculated by the following equation: gap =  $1240/\lambda_{\rm onset}$  of the polymer film. <sup>e</sup>Calculated from cyclic voltammetry (potentials vs Ag/AgCl) using 0.1 M TBAPF<sub>6</sub> in CH<sub>3</sub>CN as an electrolyte. Estimated from the calculated  $E_{\rm g}$  and HOMO. Estimated from thermogravimetry analysis (TGA) at 5% mass loss.

semiconducting polymer via side-chain engineering can be done in few synthetic steps and prevents the disruption of the  $\pi$ -conjugation in the polymer backbone. Finally, galactose is an abundant nontoxic carbohydrate, compatible with biobased substrates, such as cellulose or chitin, which is of particular interest for the large-scale fabrication of transient electronics. 39,40 For these reasons, several sugar-based compounds, such as sucrose and glucose, and complex macromolecules, such as paper, have been recognized as promising candidates for the fabrication of emerging green technologies.

In this work, carbohydrate-containing alkyl side chains were incorporated to conjugated polymer through glycosylation. A series of conjugated random copolymers incorporating various ratios of carbohydrate-containing blocks were then synthesized to evaluate the influence of the carbohydrate content onto the solid-state morphology and physical properties (including solubility in eco-friendly solvents) of the  $\pi$ -conjugated materials. The resulting materials were shown to become soluble in alcohol-based solvents upon addition of ≥20 mol % carbohydrate side chains. After complete characterization of the materials by atomic force microscopy (AFM), grazingincidence wide-angle X-ray scattering (GIWAXS), and optical spectroscopies, the new materials were directly utilized for the fabrication of organic field-effect transistors with eco-friendly solvents. Given the synthetic tunability of the side-chain engineering approach and the impact on the final solubility, the utilization of carbohydrate moieties for the design of new  $\pi$ conjugated polymer is a particularly efficient strategy to finetune the solid-state, charge transport, and optoelectronic properties of  $\pi$ -conjugated semiconducting polymers.

## ■ RESULTS AND DISCUSSION

The synthetic route to the carbohydrate-containing poly-(isoindigo-thiophene) random copolymer is depicted in Scheme 1. Starting from dibromoisoindigo, alkylation with 9bromo-1-nonanol is performed in basic conditions to afford compound 1 (35% yield). It is important to note that 9-bromo-1-nonanol was chosen as an alkyl spacer to minimize steric hindrance. This spacer length is sufficient to allow for the

isoindigo core and the galactose pendant groups to move independently of one another and minimize aggregation. Additionally, a longer spacer can favor stacking of the polymer backbones, enhance solid-state planarity, and avoid odd-even effects. 41,42 The hydroxy-terminated isoindigo derivative is then reacted with  $\beta$ -D-galactose pentaacetate in the presence of boron trifluoride diethyl etherate to afford acetyl-protected galactose-containing isoindigo monomer 2 in 42% yield. To ensure good solubility of the monomers in the reaction mixture, polymerization was directly performed via Stille coupling with various ratios of (E)-6,6'-dibromo-1,1'-bis(2decyltetradecyl)-[3,3'-biindolinylidene]-2,2'-dione and bis-(trimethylstannyl)thiophene to afford acetyl-protected random copolymers P1a to P4a, with carbohydrate ratios ranging from 0 to 80 mol %. The resulting conjugated polymers with varied ratios of carbohydrate-containing side chains were purified by successive Soxhlet extractions. In a final step, the acetylprotected conjugated polymers were deprotected using sodium hydroxide and methanol to access galactose-containing polymers P1b to P4b, with carbohydrate ratios ranging from 0 to 80 mol %. Since the solubility of the resulting deprotected polymers is significantly different upon addition of carbohydrate side chains, the resulting polymers were purified by multiple precipitation in cold methanol. A detailed experimental procedure for the preparation of P1b to P4b is described in the Supporting Information. Notably, the preparation and deprotection of a fully glycosylated polymer (P5) were also performed as detailed in the Supporting Information. However, the resulting deprotected material showed poor solubility in common organic solvents due to its extensive hydrogen bonding and the lack of solubilizing alkyl side chains, preventing further characterizations.

To confirm the structures of P1a to P4a, <sup>1</sup>H NMR at 100 °C in deuterated 1,1,2,2-tetrachloroethane (TCE- $d_2$ ) was performed. As shown in Figure S1, variable-temperature NMR was utilized to confirm the ratios of carbohydrate-containing blocks, which can differ from the feed ratios used for the preparation of the polymers. This analysis was performed by comparison of the signal related to the carbohydrate moieties

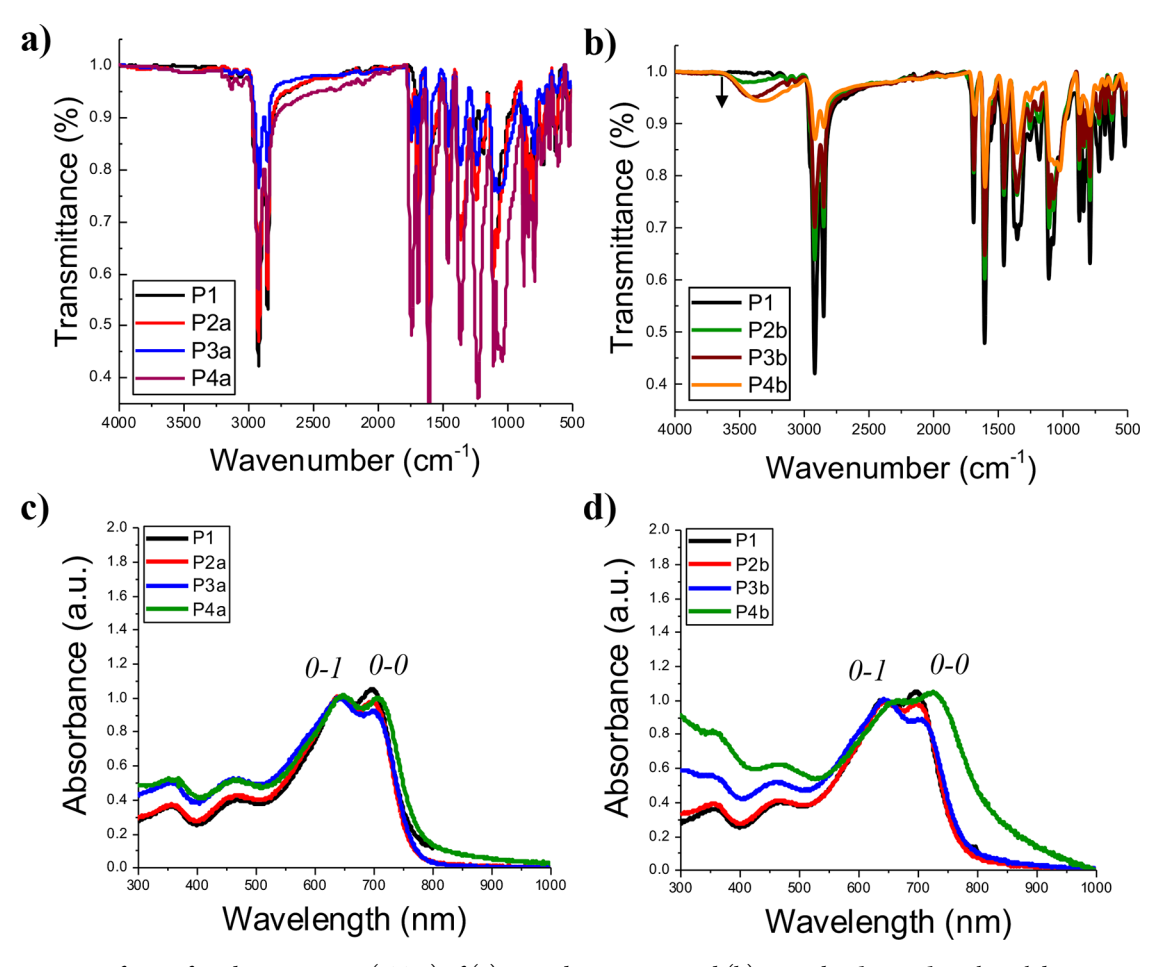


Figure 1. Fourier transform infrared spectroscopy (FTIR) of (a) P1 and P2a to P4a and (b) P1 and P2b to P4b in the solid-state; UV—vis spectra of (c) P1 to P4a and (d) P1 to P4b in the thin film casted on SiO<sub>2</sub>.

(peak at  $\delta$  = 4.2 ppm) with that of the lactam ring of isoindigo (peak at  $\delta = 3.9$  ppm). Upon confirmation of their chemical structures, the new polymers were characterized through various methods, with the results summarized in Table 1. The acetyl-protected polymers (P1a to P4a) were found to have moderate molecular weights, as measured by high-temperature size-exclusion chromatography (SEC). The progressive decrease in the average molecular weight upon incorporation of the carbohydrate-containing side chains can be directly attributed to the impact of the side chains on polymer solubility in the organic solvents used in Stille cross-coupling polymerization, which cause the polymer to precipitate out of solution during polymerization, leading to lower molecular weights. Despite this occurrence, previously observed for similar conjugated polymers designed through side-chain engineering,  $^{43,44}$  the number-average molecular weights  $(M_n)$ remained in a similar range of values even with the increasing ratio of carbohydrate side chains. As shown in Figures S2 and S3, the HOMO/LUMO levels and bandgap were evaluated by UV-vis spectroscopy and cyclic voltammetry. Additionally, thermogravimetric analysis (Figure S4) was utilized to determine the thermal decomposition temperatures (measured at 5% weight loss). All polymers showed a thermal decomposition above 300 °C, which confirms that the incorporation of galactose does not significantly affect the thermal stability.

Upon synthesis of a series of isoindigo-based random copolymers with acetyl-protected galactose moieties incorpo-

rated on the side chain, the deprotection of the carbohydrate alcohol groups was performed in basic conditions to access fully deprotected, polar semiconducting polymers. To confirm the deprotection of the acetyl group, the disappearance of the acetyl protecting groups was monitored by Fourier transform infrared spectroscopy (FTIR), and the results are summarized in Figure 1 and Figure S5. Due to the absence of ester groups in the deprotected polymers, the signal associated with the protecting acetyl groups can be used to monitor the deprotection. P2a to P4a, incorporating protected galactose, showed a distinct peak at 1740 cm<sup>-1</sup>, which correlates to the ester moieties. The relative intensity of this peak was also directly correlated to the amount of side chain containing the polymer. As shown in Figure 1a,b and Figure S5, this characteristic peak completely disappears upon removal of the acetyl groups, thus confirming the successful deprotection of the semiconducting polymers. Notably, the deprotection of the acetyl groups did not influence the molecular weights for P1b to P4b, which remain similar to the protected polymers. Additionally, FTIR can be used to qualitatively identify hydrogen-bonding by monitoring the O-H stretching peak associated with intermolecularly bonded alcohols at 3400 cm<sup>-1</sup>. 44,45 As the ratio of the galactose-containing monomer increases from P1 to P4b, the intensity of this peak also increases, as shown by the arrow in Figure 1b. The presence of intermolecular hydrogen bonding between the polymer chains can potentially explain this increase in intensity and the shift in

the wavenumber observed at higher ratios of carbohydrate side

To further probe the influence of the galactose moieties on the optoelectronic properties of the conjugated polymers, UV-vis spectroscopy was utilized in thin films (Figure 1c,d and Figure S2). Importantly, a broad absorption band, centered at  $\lambda = 680$  nm, is observed for all polymers before and after deprotection, which can be attributed to the donoracceptor charge transfer in the  $\pi$ -conjugated backbone. This band not only confirms that the deprotection of the carbohydrate moieties did not affect the  $\pi$ -conjugation but also can provide some information about molecular aggregation in the solid state by looking at the intensity of two vibrational peaks (0-0 and 0-1).46 The incorporation of acetyl-protected carbohydrates progressively reduced the intensity of the 0-0 peak to reach a minimum at 50 mol % (P3a). As observed for other conjugated polymer systems, this can be correlated to a progressive decrease in aggregation caused by the bulky side chain.<sup>47</sup> More importantly, when 80 mol % carbohydrate-containing side chain was used (P4a), the intensity of this peak increase significantly, demonstrating an increase in aggregation. This is the result of fewer solubilizing alkyl side chains, which cannot prevent aggregation despite the presence of the carbohydrate moieties. A comparison of the spectra in Figure 1c,d also demonstrates that the removal of the acetyl protecting groups does not significantly affect the molecular aggregation. This result indicates that, despite the possible formation of intermolecular hydrogen bonds between the side chains, molecular aggregation is not significantly influenced by the presence of the free hydroxyl group on the carbohydrate moieties. This also confirms the important role of the solubilizing side chains in solubility and aggregation in the solid state. However, a red-shift in  $\lambda_{max}$  of increasing magnitude can be seen when comparing the protected and deprotected series going from P2 to P4 (Table 1). This trend can be attributed to the increasing presence of hydrogen bonding.

Following the initial characterization of the physical properties of the new galactose-containing poly(isoindigo) polymers, their solubilities in several eco-friendly polar solvents were carefully evaluated. To select the solvents for this investigation, two main parameters were considered: (i) the environmental and human health impacts and (ii) the compatibility with device printing methods. First, minimizing the environmental and health impacts of the solvents used in device preparation and processing is critical to the development of sustainable technologies.<sup>48</sup> Among the large variety of solvents available, we identified four alcohol-based solvents, namely, methanol, ethanol, i-propanol, and n-butanol, given their low environmental impact and minimal effects on human health. Among the possible ester or ketone-based solvents, ethyl acetate and acetone were also selected for similar reasons. All of these solvents are also commonly used in research and industry. Finally, given the general good solubility of conjugated polymers in aromatic solvents, o-anisole was also investigated as this specific solvent has much lower impacts than more commonly used toluene and chlorobenzene. Second, the printing compatibility was also considered for the selection of the solvents. 49,50 Some important printing processes, such as flexography, screen printing, gravure, or inkjet printing, have important restrictions regarding organic solvents. For example, for flexography, no aromatic or chlorinated solvents can be used given the limited compatibility of the printing plates for these solvents. Instead, alcohols

with a maximum of 20% ester are generally used. For inkjet printing, solvents with boiling points below 100 °C are privileged to avoid cavitation. Considering these limitations, we found that the list of solvents previously identified as low impacting is compatible with most large-scale printing

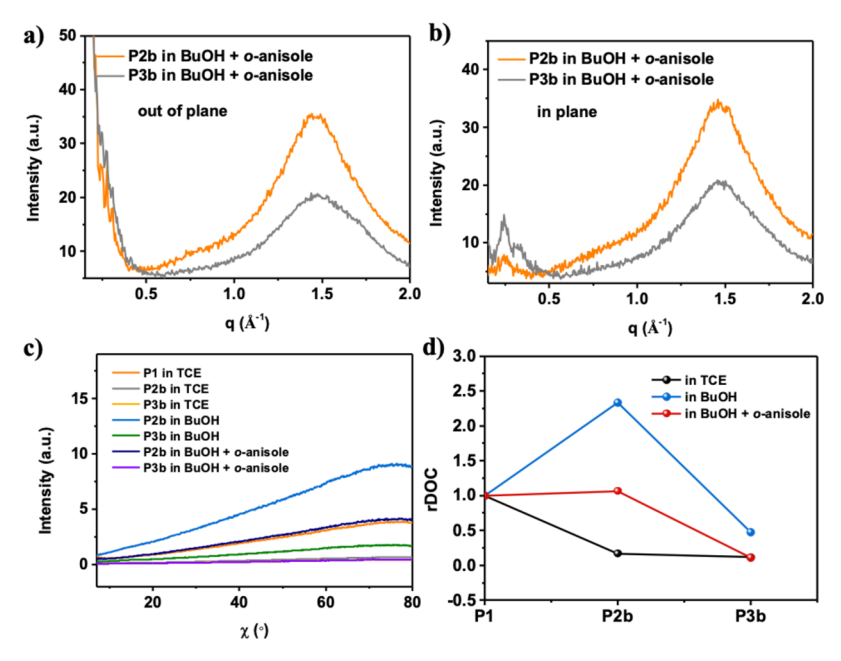
After this careful selection process, the solubilities of polymers P1b to P4b were evaluated, with the results are summarized in Table 2. To evaluate solubility, each semi-

Table 2. Solubility of Semiconducting Polymers P1 to P4b in Various Polar Solvents

solvent	P1	P2b	P3b	P4b
methanol	I	I	I	PS
ethanol	I	PS	PS	I
i-propanol	I	PS	S	S
n-butanol	I	S	S	S
acetone	I	PS	PS	I
ethyl acetate	PS	S	S	PS
o-anisole	S	S	PS	PS

<sup>a</sup>Observations for solution at 5 mg/mL: I = insoluble upon heating, S = soluble, PS = partially soluble upon heating.

conducting polymer sample was mixed in the selected solvent at a concentration of 5 mg/mL and left to stir overnight under mild heating. As expected, the incorporation of galactosecontaining side chains to the  $\pi$ -conjugated polymer significantly influenced the solubility of the polymer. P1, containing no carbohydrate, was shown to be slightly soluble in ethyl acetate and soluble in o-anisole. This result was expected since only solvents capable of disrupting the strong intermolecular  $\pi$ - $\pi$  interactions and side-chain interdigitation are typically able to solubilize rigid, semicrystalline polymers. In contrast, P2b, incorporating 20 mol % galactose-containing side chains, shows an increased solubility in many polar solvents, including alcohols, acetone, and ethyl acetate. This can be explained by the increased ratio of free hydroxyl moieties in the side chains that can interact with the polar solvent molecules and help improve solubility. However, at 20 mol %, the solubility is still suboptimal in most alcohols, mostly due to the dominance of  $\pi$ - $\pi$  interactions between the polymer chains, which prevent a complete solubilization of the macromolecules. Upon incorporation of 50 mol % carbohydrate, the influence of the free hydroxyl moieties on the polymer becomes great enough to allow for a complete solubilization of the polymer in many alcohol-based solvents such as *n*-butanol and isopropyl alcohol. Solubilities in ethanol and acetone are also significantly increased. To further fine-tune the solubilities of the semiconducting polymers in polar solvents, P4b with 80 mol % was also evaluated. Interestingly, these two polymers, despite showing an increase in solubilities in polar solvents in comparison to reference polymer P1, suffered from a significantly reduced solubility when compared to P3b. While P4b demonstrated comparable solubility to P3b in alcohol-based solvents, solubilities in other polar solvents, such as acetone and ethyl acetate, were reduced. This result confirms that, upon addition of galactose-containing side chains beyond a certain threshold, the intermolecular hydrogen bonding between the polymer side chains becomes too strong and ultimately negatively impacts the ability of the solvents to solubilize the polymer side chains. Nonetheless, this evaluation of the solubility clearly demonstrates the capability of



**Figure 2.** 1D sector-averaged profiles of **P2b** and **P3b** in (a) out-of-plane and (b) in-plane direction processed in *n*-BuOH with *o*-anisole. (c) Normalized pole figure analysis based on the (100) peak and (d) the relative degrees of crystallinity (rDoCs) of **P1**, **P2b**, and **P3b** in various solvents obtained by integrating the area below each curve from panel (c).

galactose-containing side chains to improve and tune the solubility of the conjugated polymer in eco-friendly, printing-compatible, alcohol-based solvents.

Due to their improved solubilities in alcohol-based solvents, P2b and P3b were chosen for further characterizations to compare with reference polymer P1. 1,1,2,2-Tetrachloroethane (TCE) and n-butanol (n-BuOH) were initially chosen as solvents to compare thin-film formation in common halogenated (TCE) and greener alcohol-based (n-BuOH) conditions. Importantly, it was observed that n-BuOH cannot effectively disrupt the polymer backbone aggregation to produce uniform thin films for characterization and device fabrication. Therefore, a small amount of o-anisole was used as the additive to break up the chain aggregation induced by intermolecular  $\pi$  stacking and improve film formation. Further characterizations were performed on thin films processed in TCE, n-BuOH, and a n-BuOH/o-anisole mixture to determine the thin-film morphologies of P1, P2b, and P3b and demonstrate how the chosen processing conditions affect

Grazing-incidence wide-angle X-ray scattering (GIWAXS) was carried out to understand the molecular packing and crystallite characteristics of P1, P2b, and P3b in halogenated and greener solvents. 2D scattering patterns and the corresponding 1D sector-averaged profiles (both out-of-plane and in-plane directions) are shown in Figure 2 and Figures S6-S8. The key parameters of molecular packing are summarized in Table 3. All polymers casted from TCE showed relatively weak lamellar packing peaks and an unclear  $\pi$ - $\pi$  stacking peak (Figure S6). With the increasing fraction of galactose-containing side chains, the (100) peak position remained consistent, while the peak became broader with a full width at half-maximum (FWHM) value increasing from 0.06 to 0.10 to 0.28 Å<sup>-1</sup>, indicating more broadly distributed sidechain packing. Such behavior could be the result of steric hindrance from the galactose moieties. For the polymers casted in n-BuOH, the (100) lamellar packing became more

Table 3. Crystallographic Parameters for P1, P2b, and P3b in TCE, n-BuOH, and n-BuOH with an o-Anisole Additive

polymer	(100) lamellar spacing (Å)	(100) peak FWHM (Å <sup>-1</sup> )	(1'00) lamellar spacing (Å)
P1 (TCE)	26.18	0.06	
P2b (TCE)	24.17	0.10	
P3b (TCE)	26.18	0.28	
P2b (n-BuOH)	25.13	0.06	
P3b (n-BuOH)	25.13	0.06	19.04
P2b (30% o-anisole/n-BuOH)	24.17	0.07	
P3b (10% o-anisole/ n-BuOH)	25.13	0.07	18.48

pronounced and well-defined, while a *d*-spacing of approximately 25 Å is similar to the polymers casted in TCE (Figure S7). The polymers casted in *n*-BuOH with an *o*-anisole additive also demonstrated a similar *d*-spacing, indicating that both the solvent choice and the galactose fraction do not significantly affect the alkyl side-chain packing distance.

Interestingly, P3b showed a separate (100) peak corresponding to a *d*-spacing of approximately 19 Å in both *n*-BuOH and *n*-BuOH with an *o*-anisole additive, which is likely the result of the stronger H-bonding interactions between adjacent carbohydrate groups in alcohol-based processing (Figures S7b and S8b). Since the lamellar spacing is a measure of side-chain packing, the two distinct peaks correspond to the spacing between the two different side chains (alkyl and carbohydrate) that are present in equal amounts in P3b. The strong H-bonding between the galactose-containing side chains that do not interact in the same manner with one another. This second peak is not present in P2b because there are significantly fewer galactose-containing side chains to interact with one another, enough to affect side-chain packing.

To provide a better understanding of the polymer crystallites, the relative degree of crystallinity (rDoC) was

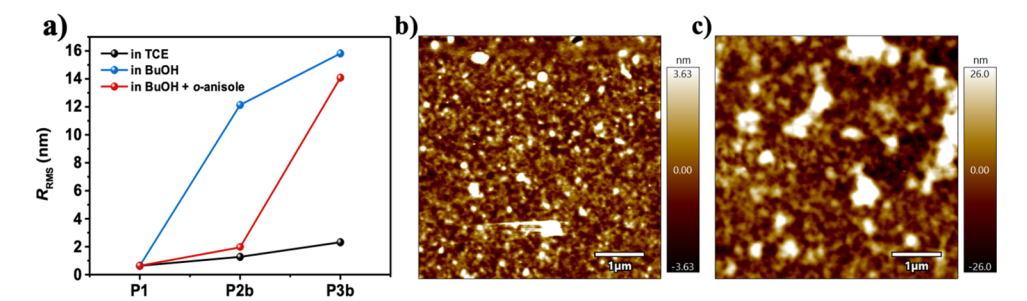


Figure 3. (a) Root-mean-square (RMS) surface roughness for P1, P2b, and P3b in TCE, n-BuOH, and n-BuOH with an o-anisole additive. AFM height images for (b) P2b and (c) P3b in n-BuOH with an o-anisole additive. The scale bar is 1  $\mu$ m.

also analyzed based on the pole figure extracted from the (100) peak (Figure 2c). For the relative degree of crystallinity, a plot of intensity versus the azimuthal angle  $(\chi)$  was first obtained based on the (100) peak. Next, a normalized intensity was calculated by dividing the intensity by exposure time, sample thickness, and the length of the beam path. Then, a geometrically corrected orientation distribution function was performed  $(\sin(\chi)I(\chi))$  to obtain the scattering intensity for crystals with different orientation distributions. The relative degree of crystallinity is obtained by integrating total scattering intensity (or the area below the scattering intensity vs scattering angle curve) followed by comparison with other samples. The detailed procedure can be found elsewhere. 52,53 As depicted in Figure 2d, for the polymers casted in TCE, the rDoC decreased continuously with increasing galactosecontaining side-chain content, while P2b and P3b showed approximately 8 times less crystallinity than P1. On the other hand, P2b casted from n-BuOH showed 2 times higher crystallinity than P1, which may also come from the stronger H-bonding interactions between carbohydrate groups, leading to better aggregation. This observation is in agreement with the result from UV-vis spectroscopy. Upon the addition of oanisole, the pole figure areas of both P2b and P3b decrease, (Figure 3c), suggesting that the addition of o-anisole helps to disrupt the solution-state aggregation of the polymers and increases the solubility effectively.

Atomic force microscopy (AFM) was also used to investigate the surface morphologies of P1, P2b, and P3b (Figure 3 and Figure S9). All three polymers casted in TCE showed relatively smooth surfaces with a nanofibrillar structure compared with those casted in *n*-BuOH (Figure S9). With the increased fraction of carbohydrate groups, the thin-film surface got slightly rougher ( $R_{RMS} = 0.65$ , 1.30, and 2.32 nm for P1, P2b, and P3b in TCE). For the polymers casted in n-BuOH, the roughness increased more dramatically, up to 14 nm for P3b (Figure 3a). However, the roughness decreased significantly upon the addition of the solvent additive, oanisole, which verified its capability of breaking polymer aggregates in solution (Figure 3a).

Upon characterization of the new carbohydrate-containing isoindigo-based polymers and the evaluation of their optoelectronic properties and solid-state morphology in chlorinated and eco-friendly solvents, the new materials were used for the production of organic field-effect transistors (OFETs). Devices with bottom-gate top-contact configurations were fabricated with P2b and P3b, and the results were compared with reference polymer P1. A chlorinated solvent (1,1,2,2-tetrachloroethane, TCE) and a greener solvent mixture (o-anisole in n-BuOH) were used for the fabrication

of the devices, with the experimental procedure detailed in the Supporting Information. Briefly, the polymer was dissolved in the selected solvent (3 mg/mL) and stirred overnight upon mild heating. The solution was then spin-coated at 1000 rpm onto a Si/SiO2 wafer, functionalized with n-octadecyltrichlorosilane (OTS).54 Gold electrodes were then deposited on the substrate through physical vapor deposition. As shown in Figures S10-S12, transfer and output curves were measured for all polymers. The charge carrier mobility was extracted from the transfer curves through linear fitting of the  $I_{DS}^{-1/2}$ versus  $V_{\rm GS}$  curves in the saturation regime, using the following equation:  $I_{DS(sat)} = (WC/2L)\mu_{sat}(V_G - V_{th})^2$ . The results obtained from the fabrication of OFETs are summarized on Table 4. It is important to note that the transfer and output

Table 4. Average and Maximum Hole Mobilities ( $\mu_h^{ave}$ ,  $\mu_{\rm h}^{\rm max}$ ), Threshold Voltages  $(V_{\rm th})$ , and  $I_{\rm on}/I_{\rm off}$  Current Ratios for OFETs Fabricated from Semiconducting Polymers P1, P2b, and P3b in 1,1,2,2-Tetrachloroethane (TCE) and n-Butanol (n-BuOH) with the o-Anisole Additive<sup>a</sup>

polymer	thickness $(nm)^b$	W/L	$(10^{-4} \text{ cm}^2 \text{ V}^{-1} \text{ s}^{-1})$	$I_{\rm ON}/I_{\rm OFF}^{\rm \ \ ave}$	$V_{ m th}^{ m ave} \  m (V)$
P1 (TCE)	40-50	20	$1.91 \pm 0.55/2.60$	$10^{4}$	-21.7
P1 (30% o- anisole/n -BuOH)	N/A	N/A	N/A	N/A	N/A
P2b (TCE)	40-50	20	$2.29 \pm 0.62/3.22$	$10^{5}$	-17.3
P2b (30% o- anisole/n -BuOH)	40-50	20	$1.27 \pm 0.30/1.72$	10 <sup>5</sup>	-26.2
P3b (TCE)	40-50	20	$0.373 \pm 0.02/0.401$	$10^{4}$	-20.2
P3b (10% o- anisole/n -BuOH)	40-50	20	$0.240 \pm 0.03/0.266$	10 <sup>3</sup>	-22.6

<sup>a</sup>Results are averaged from five devices and acquired after thermal annealing at 150 °C. <sup>b</sup>Thickness measured by AFM.

curves slightly deviate from ideal device characteristics, especially for P3b that contains a greater ratio of polar moieties. Nonetheless, all devices presented curves scaled in the form of  $I_{\rm DS} \sim (V_{\rm G} - V_{\rm T})^{1/2}$  within the mobility extraction

Initial evaluation of the charge mobility of P1 was first performed in TCE. Despite showing good solubility in chlorobenzene, a more common organic solvent used for OFET fabrication, TCE was chosen to build up a reliable comparison with P2b and P3b, which have a better solubility in this solvent. When processed from TCE, P1 showed an average mobility of  $1.91 \times 10^{-4} \text{ cm}^2 \text{ V}^{-1} \text{ s}^{-1}$  after thermal annealing. Despite being lower than other  $\pi$ -conjugated polymers based on isoindigo, the measured mobility is very comparable to previously reported values for similar materials. 55,56 Importantly, no working device was obtained for P1 in n-BuOH due to the low solubility preventing film formation. P2b, containing 20 mol % carbohydrate-containing side chains, was evaluated in OFETs using both TCE and n-BuOH. Given the strong  $\pi - \pi$  interactions, a small amount of o-anisole (30%), a greener aromatic solvent, was added to n-BuOH to prevent backbone aggregation. Interestingly, P2b showed an average mobility of  $1.27 \times 10^{-4}$  cm<sup>2</sup> V<sup>-1</sup> s<sup>-1</sup>, a value similar to that measured for P1 in TCE. Devices prepared from the same polymer in TCE showed a similar average mobility (2.29 × 10<sup>-4</sup> cm<sup>2</sup> V<sup>-1</sup> s<sup>-1</sup>). This result demonstrates that not only the introduction of carbohydrate side chains does not largely impact the charge transport but also confirm that this sidechain engineering approach is efficient for transitioning the processing of  $\pi$ -conjugated polymers from chlorinated solvents to greener solvents such as n-BuOH and o-anisole. For P3b, incorporating 50 mol % carbohydrate-containing side chains, average mobilities of  $0.373 \times 10^{-4}$  and  $0.273 \times 10^{-4}$  cm<sup>2</sup> V<sup>-1</sup> s<sup>-1</sup> were measured for devices built from TCE and n-BuOH, respectively. Importantly, to get a smooth film in butanol, 10% o-anisole was added to process P3b. In contrast to the devices prepared from P2b, an increased content of o-anisole resulted in poor film formation. This result confirms that, at a higher amount of carbohydrate, the polymer becomes more polar due to the formation of more intermolecular hydrogen bonding. Therefore, the green solvent mixture needs to be adjusted to decrease the backbone aggregation through  $\pi$ -stacking while maintaining a good solubility in n-BuOH. Similarly, as what has been observed for P2b, mobility values obtained for devices fabricated from greener solvents are similar to those obtained from TCE. It is important to note that no working devices were achieved for P4b (80 mol % carbohydratecontaining side chains). This can be explained by the increased number of intermolecular hydrogen bonds as the amount of carbohydrate increases, ultimately negatively impacting the solubility of the conjugated polymer in chlorinated, aromatic, and alcohol-based organic solvents.

# CONCLUSIONS

In summary, novel  $\pi$ -conjugated polymers based on isoindigo, and incorporating carbohydrate-containing side chains, were prepared. Stille polymerization was utilized to prepared random copolymers with different amounts of acetyl-protected carbohydrate-containing side chains (from 0 to 100 mol %). In a following step, the acetyl-protected conjugated polymers were deprotected under mild conditions to achieve galactosecontaining polymers, and a systematic evaluation of their solidstate morphology and optoelectronics properties was performed using various characterizations such as UV-vis spectroscopy, AFM, and GIWAXS. The presence of galactose moieties in the side chains was shown to increase aggregation in solution and the solid state. More importantly, the progressive addition of the polar side chains significantly influenced the solubility of the materials in green organic solvents. P1, containing no carbohydrate, was shown to be slightly soluble in ethyl acetate and soluble in o-anisole. In contrast, P2b and P3b, incorporating, respectively, 20 and 50 mol % galactose-containing side chains, showed an increased solubility in many polar solvents, including alcohols, acetone, and ethyl acetate, attributed to the free hydroxyl moieties in the side chains that can interact with the polar solvent molecules and help improve solubility. Upon further addition

of carbohydrate in the side chains of the  $\pi$ -conjugated polymers, solubilities in polar solvents were reduced due to the formation of an extensive network of intermolecular hydrogen bonds between the carbohydrate-containing polymers. To evaluate charge transport in the selected green solvents, P2b and P3b were used as semiconductors for the fabrication of OFETs. Both polymers showed similar charge transport properties to the reference polymer P1 when processed in a high boiling point solvent. Importantly, both polymers also showed comparable field-effect charge mobilities when processed from a mixture of green solvents (n-BuOH/oanisole), which was not possible for the reference polymer due to its poor solubility in green solvents. This result confirms that carbohydrate side chains are an efficient strategy to fine-tune the solubility of  $\pi$ -conjugated polymers in greener solvents without sacrificing charge transport. Additionally, the new ecofriendlier semiconducting polymers are promising candidates for the fabrication of thin-film devices through large-scale deposition techniques, which are typically incompatible with high-boiling-point chlorinated solvents. Traditionally used in medicinal and biopharmaceutic chemistry, carbohydrates are a powerful design element to consider achieving greener materials, ultimately offering a sustainable solution to reduce electronic waste accumulation.

## **■ EXPERIMENTAL SECTION**

**Materials.** Commercial reactants were used without further purification unless stated otherwise. All the solvents used in these reactions were distilled prior to use. The tris(dibenzylideneacetone)-dipalladium(0)-chloroform adduct  $(Pd_2(dba)_3 \cdot CHCl_3)$  was purchased from Sigma-Aldrich and recrystallized following a reported procedure. <sup>57</sup> (E)-6,6'-Dibromo-1,1'-bis(2-decyltetradecyl)-[3,3'-biin-dolinylidene]-2,2'-dione was synthesized according to the literature. <sup>42</sup>

Measurements and Characterization. Nuclear magnetic resonance (NMR) spectra were recorded on a Bruker 300 MHz. The spectra for all polymers were obtained in deuterated 1,1,2,2tetrachloroethane (TCE-d<sub>2</sub>) at 100 °C. Chemical shifts are given in parts per million (ppm). Number average molecular weight  $(M_n)$ , weight average molecular weight  $(M_w)$ , and dispersity (D) were evaluated by high-temperature size exclusion chromatography (SEC) using 1,2,4-trichlorobenzene and performed on an EcoSEC HLC-8321GPC/HT (Tosoh Bioscience) equipped with a single TSK gel GPC column (GMHHR-H; 300 mm × 7.8 mm) calibrated with monodisperse polystyrene standards. The samples were prepared using 1 mg/mL of sample in trichlorobenzene (TCB), which were allowed to stir at 80 °C for 12 h prior to injection. The analysis of the samples was performed at 180 °C with a flow rate of 1.0 mL/min with injection quantities of 300 µL. The data was collected and integrated using an EcoSEC 8321GPC HT software suite. UV-vis spectroscopy was performed on a Varian UV-vis Cary 50 spectrophotometer. The surface structure of the polymer film was obtained using a multimode atomic force microscope (Asylum Cypher) operated in the tapping mode at room temperature. All electrical measurements were conducted using a Keithley 4200 semiconductor parameter analyzer (Keithley Instruments Inc.) under dry N<sub>2</sub> (glovebox). Film thickness was evaluated by AFM. GIWAXS performed on a laboratory beamline system (Xenocs Inc. Xeuss 2.0) with an X-ray wavelength of 1.54 Å. An incidence angle of 0.2° was used. Samples were kept under vacuum to minimize air scattering. Diffraction images were recorded on a Pilatus 1M detector (Dectris Inc.) with an exposure time of 1.5 h and processed using a Nika software package, in combination with WAXSTools.58

**Evaluation of Solubility.** Vials equipped with magnetic stir bars were charged with 1 mL of the desired solvent and 5 mg of a poly(isoindigo) derivative. The vials were then heated to 60  $^{\circ}$ C and stirred for 24 h. Solubility was determined visually using the following definitions: a polymer was defined as "soluble" when no solid

remained in solution, "partially soluble" when the solvent was colored but small amounts of solid remained in solution, and "insoluble" when the solvent remained colorless and all polymer remained solid.

Device Fabrication. Bottom-gate top-contact (BGTC) OFET devices were fabricated on a highly doped n-type Si(100) wafer with a 300 nm-thick SiO<sub>2</sub> dielectric layer. Wafers were first functionalized with an n-octadecyltrimethoxysilane (OTS) self-assembled monolayer, according to the reported method. The OTS-treated substrate was washed with toluene, acetone, and isopropanol and then dried with nitrogen before use. Thin films of the polymer blends were spincast at 1000 rpm onto OTS-treated substrates from prepared polymer solutions (3 mg mL<sup>-1</sup>) giving films approximately 50  $\mu$ m thick. A gold source and drain contacts were then deposited through a shadow mask via e-beam physical vapor deposition. 50 nm of Au (2 Å s<sup>-1</sup>) was deposited on top of the polymer films, yielding devices with channel length L and width W defined as 150 and 1000  $\mu$ m, respectively. Thermal annealing was carried out using a hot plate at 150 °C inside a glove box under an N<sub>2</sub> atmosphere. Measurements of the device characteristics were conducted at room temperature using a Keithley 4200-SCS semiconductor parameter analyzer (Keithley Instruments Inc., Cleveland, OH, USA) inside a N2-purged glovebox.

#### ASSOCIATED CONTENT

## Supporting Information

The Supporting Information is available free of charge at https://pubs.acs.org/doi/10.1021/acsami.1c02860.

General procedure and materials; method for solubility determination; procedures for device fabrication and sample preparation; synthetic methods and NMR spectra; polymers composition by <sup>1</sup>H NMR spectroscopy; UV-vis spectra of P1-P4 before and after deprotection; cyclic voltammograms of P1-P4; thermogravimetric analyses of P1-P4; Fourier transform infrared spectra of P1a to P4a and P1b to P4b; 2D GIWAXS scattering patterns of P1, P2b, and P3b; sector-averaged 1D GIWAXS profiles for P1, P2b, and P3b; AFM height images of P1, P2b, and P3b in TCE and n-BuOH; output curves of P1, P2b, and P3b in TCE and *n*-butanol/o-anisole; transfer curves of P1, P2b, and P3b in TCE and n-butanol/o-anisole; transfer curves of P1, P2b, and P3b showing hysteresis behavior (PDF)

#### AUTHOR INFORMATION

## **Corresponding Authors**

Xiaodan Gu — School of Polymer Science and Engineering, The University of Southern Mississippi, Hattiesburg, Mississippi 39406, United States; orcid.org/0000-0002-1123-3673; Email: Xiaodan.Gu@usm.edu

Simon Rondeau-Gagné — Department of Chemistry and Biochemistry, University of Windsor, Windsor, Ontario N9B 3P4, Canada; orcid.org/0000-0003-0487-1092; Email: srondeau@uwindsor.ca

## Authors

Madison Mooney – Department of Chemistry and Biochemistry, University of Windsor, Windsor, Ontario N9B 3P4, Canada

Yunfei Wang — School of Polymer Science and Engineering, The University of Southern Mississippi, Hattiesburg, Mississippi 39406, United States; orcid.org/0000-0001-7555-5308

Audithya Nyayachavadi – Department of Chemistry and Biochemistry, University of Windsor, Windsor, Ontario N9B 3P4, Canada Song Zhang — School of Polymer Science and Engineering, The University of Southern Mississippi, Hattiesburg, Mississippi 39406, United States; orcid.org/0000-0001-9815-7046

Complete contact information is available at: https://pubs.acs.org/10.1021/acsami.1c02860

#### **Author Contributions**

All authors contributed to the manuscript. All authors have given approval to the final version of the manuscript.

#### Funding

This work was supported by NSERC through a Discovery Grants (RGPIN-2017-06611) and the NSERC Green Electronics Network (GreEN) (NETGP 508526-17). S.R.-G. also acknowledges the Canada Foundation for Innovation (CFI), the Ontario Research Fund, and the University of Windsor for financial support. M.M. thanks NSERC for financial support through a Canada Graduate Scholarship—Master. M.M. and A.N. thank NSERC for financial support through a Canada Postgraduate Scholarship—Doctoral. S.Z. thanks NSF office of integrative activities for support under award number of OIA-1757220. Y.W. and X.G. thank the financial support from the U.S. Department of Energy, Office of Science, Office of Basic Energy Science under award number of SC0019361 for supporting the scattering portion of this work. The authors declare no competing financial interest.

#### **Notes**

ı

The authors declare no competing financial interest.

## ACKNOWLEDGMENTS

The authors thank Jean-François Morin and his group (U. Laval) for MS measurements and Lara Watanabe (U. Windsor) for elemental analysis.

#### REFERENCES

- (1) Gubbi, J.; Buyya, R.; Marusic, S.; Palaniswami, M. Internet of Things (IoT): A Vision, Architectural Elements, and Future Directions. Future Gener. Comput. Syst. 2013, 29, 1645–1660.
- (2) Zhan, Y.; Mei, Y.; Zheng, L. Materials Capability and Device Performance in Flexible Electronics for the Internet of Things. *J. Mater. Chem. C* **2014**, *2*, 1220–1232.
- (3) Swan, M. Sensor Mania! The Internet of Things, Wearable Computing, Objective Metrics, and the Quantified Self 2.0. *J. Sens. Actuator Netw.* **2012**, *1*, 217–253.
- (4) Ahn, J.-H.; Je, J. H. Stretchable Electronics: Materials, Architectures and Integrations. J. Phys. D: Appl. Phys. 2012, 45, 103001.
- (5) Hua, Q.; Sun, J.; Liu, H.; Bao, R.; Yu, R.; Zhai, J.; Pan, C.; Wang, Z. L. Skin-Inspired Highly Stretchable and Conformable Matrix Networks for Multifunctional Sensing. *Nat. Commun.* **2018**, *9*, 244.
- (6) Zeng, W.; Shu, L.; Li, Q.; Chen, S.; Wang, F.; Tao, X. M. Fiber-Based Wearable Electronics: A Review of Materials, Fabrication, Devices, and Applications. *Adv. Mater.* **2014**, *31*, 5310–5336.
- (7) Hammock, M. L.; Chortos, A.; Tee, B. C.-K.; Tok, J. B.-H.; Bao, Z. 25th Anniversary Article: The Evolution of Electronic Skin (e-Skin): A Brief History, Design Considerations, and Recent Progress. *Adv. Mater.* **2013**, 25, 5997–6038.
- (8) O'Connor, T. F.; Rajan, K. M.; Printz, A. D.; Lipomi, D. J. Toward Organic Electronics with Properties Inspired by Biological Tissue. *J. Mater. Chem. B* **2015**, *3*, 4947–4952.
- (9) Morin, P. O.; Bura, T.; Leclerc, M. Realizing the Full Potential of Conjugated Polymers: Innovation in Polymer Synthesis. *Mater. Horiz.* **2016**, *3*, 11–20.
- (10) Wang, G.-J. N.; Gasperini, A.; Bao, Z. Stretchable Polymer Semiconductors for Plastic Electronics. *Adv. Electron. Mater.* **2018**, *4*, 1700429–1700450.

- (11) Savagatrup, S.; Printz, A. D.; O'Connor, T. F.; Zaretski, A. V.; Lipomi, D. J. Molecularly Stretchable Electronics. *Chem. Mater.* **2014**, 26, 3028–3041.
- (12) Zhang, S.; Cheng, Y.-H.; Galuska, L.; Roy, A.; Lorenz, M.; Chen, B.; Luo, S.; Li, Y. T.; Hung, C.-C.; Qian, Z.; St. Onge, P. B. J.; Mason, G. T.; Cowen, L.; Zhou, D.; Nazarenko, S. I.; Storey, R. F.; Schroeder, B. C.; Rondeau-Gagné, S.; Chiu, Y.-C.; Gu, X. Tacky Elastomers to Enable Tear Resistant and Autonomous Self-Healing Semiconductor Composites. *Adv. Funct. Mater.* **2020**, *30*, 2000663—2000673.
- (13) St. Onge, P. B. J.; Ocheje, M. U.; Selivanova, M.; Rondeau-Gagné, S. Recent Advances in Mechanically Robust and Stretchable Bulk Heterojunction Polymer Solar Cells. *Chem. Rec.* **2019**, *19*, 1008–1027.
- (14) Oh, J. Y.; Rondeau-Gagné, S.; Chiu, Y.-C.; Chortos, A.; Lissel, F.; Wang, G.-J. N.; Schroeder, B. C.; Kurosawa, T.; Lopez, J.; Katsumata, T.; Xu, J.; Zhu, C.; Gu, X.; Bae, W.-G.; Kim, Y.; Jin, L.; Chung, J. W.; Tok, J. B.-H.; Bao, Z. Intrinsically Stretchable and Healable Semiconducting Polymer for Organic Transistors. *Nature* 2016, 539, 411–415.
- (15) Ocheje, M. U.; Charron, B. P.; Nyayachavadi, A.; Rondeau-Gagné, S. Stretchable Electronics: Recent Progress in the Preparation of Stretchable and Self-Healing Semiconducting Conjugated Polymers. *Flex. Print. Electron.* **2017**, *2*, 043002–043018.
- (16) Wen, H.-F.; Wu, H.-C.; Aimi, J.; Hung, C.-C.; Chiang, Y.-C.; Kuo, C.-C.; Chen, W.-C. Soft Poly(Butyl Acrylate) Side Chains toward Intrinsically Stretchable Polymeric Semiconductors for Field-Effect Transistor Applications. *Macromolecules* **2017**, *50*, 4982–4992.
- (17) Ocheje, M. U.; Selivanova, M.; Zhang, S.; Van Nguyen, T. H.; Charron, B. P.; Chuang, C.-H.; Cheng, Y.-H.; Billet, B.; Noori, S.; Chiu, Y.-C.; Gu, X.; Rondeau-Gagné, S. Influence of Amide-Containing Side Chains on the Mechanical Properties of Diketo-pyrrole-Based Polymers. *Polym. Chem.* **2018**, *9*, 5531–5542.
- (18) Savagatrup, S.; Printz, A. D.; O'Connor, T. F.; Zaretski, A. V.; Rodriquez, D.; Sawyer, E. J.; Rajan, K. M.; Acosta, R. I.; Root, S. E.; Lipomi, D. J. Mechanical Degradation and Stability of Organic Solar Cells: Molecular and Microstructural Determinants. *Energy Environ. Sci.* **2015**, *8*, 55–80.
- (19) O'Connor, B.; Kline, R. J.; Conrad, B. R.; Richter, L. J.; Gundlach, D.; Toney, M. F.; DeLongchamp, D. M. Anisotropic Structure and Charge Transport in Highly Strain-Aligned Regioregular Poly(3-Hexylthiophene). *Adv. Funct. Mater.* **2011**, *21*, 3697–3705.
- (20) Mercier, L. G.; Leclerc, M. Direct(Hetero)Arylation: A New Tool for Polymer Chemists. Acc. Chem. Res. 2013, 46, 1597–1605.
- (21) Pouliot, J.-R.; Sun, B.; Leduc, M.; Najari, A.; Li, Y.; Leclerc, M. A high mobility DPP-based polymer obtained *via* direct (hetero)-arylation polymerization. *Polym. Chem.* **2015**, *6*, 278–282.
- (22) Mooney, M.; Nyayachavadi, A.; Rondeau-Gagné, S. Eco-Friendly Semiconducting Polymers: From Greener Synthesis to Greener Processability. *J. Mater. Chem. C* **2020**, *8*, 14645–14664.
- (23) Desmurs, J.-R.; Ratton, S. Anisole: An Excellent Solvent. *Ind. Chem. Libr.* **1996**, *8*, 481–488.
- (24) Zhou, Y.; Gu, K. L.; Gu, X.; Kurosawa, T.; Yan, H.; Guo, Y.; Koleilat, G. I.; Zhao, D.; Toney, M. F.; Bao, Z. All-Polymer Solar Cells Employing Non-Halogenated Solvent and Additive. *Chem. Mater.* **2016**, 28, 5037–5042.
- (25) Zhu, C.; Liu, L.; Yang, Q.; Lv, F.; Wang, S. Water-Soluble Conjugated Polymers for Imaging, Diagnosis, and Therapy. *Chem. Rev.* **2012**, *112*, 4687–4735.
- (26) Traina, C. A.; Bakus, R. C., II; Bazan, G. C. Design and Synthesis of Monofunctionalized, Water-Soluble Conjugated Polymers for Biosensing and Imaging Applications. *J. Am. Chem. Soc.* **2011**, *133*, 12600–12607.
- (27) Zhao, H.; Zhu, B.; Sekine, J.; Luo, S.-C.; Yu, H.-H. Oligoethylene-Glycol-Functionalized Polyoxythiophenes for Cell Engineering: Syntheses, Characterizations, and Cell Compatibilities. *ACS Appl. Mater. Interfaces* **2012**, *4*, 680–686.

- (28) Schmatz, B.; Yuan, Z.; Lang, A. W.; Hernandez, J. L.; Reichmanis, E.; Reynolds, J. R. Aqueous Processing for Printed Organic Electronics: Conjugated Polymers with Multistage Cleavable Side Chains. ACS Cent. Sci. 2017, 3, 961–967.
- (29) Song, I.; Kim, H.-W.; Ahn, J.; Han, M.; Kwon, S.-K.; Kim, Y.-H.; Oh, J. H. Non-Halogenated Solution-Processed Ambipolar Plastic Transistors Based on Conjugated Polymers Prepared by Asymmetric Donor Engineering. J. Mater. Chem. C 2019, 7, 14977—14985.
- (30) Nguyen, T. L.; Lee, C.; Kim, H.; Kim, Y.; Lee, W.; Oh, J. H.; Kim, B. J.; Woo, H. Y. Ethanol-Processable, Highly Crystalline Conjugated Polymers for Eco-Friendly Fabrication of Organic Transistors and Solar Cells. *Macromolecules* **2017**, *50*, 4415–4424.
- (31) Chen, Z.; Yan, L.; Rech, J. J.; Hu, J.; Zhang, Q.; You, W. Green-Solvent-Processed Conjugated Polymers for Organic Solar Cells: The Impact of Oligoethylene Glycol Side Chains. *ACS Appl. Polym. Mater.* **2019**, *1*, 804–814.
- (32) Lee, J.; Kim, G.-W.; Kim, M.; Park, S. A.; Park, T. Nonaromatic Green-Solvent-Processable, Dopant-Free, and Lead-Capturable Hole Transport Polymers in Perovskite Solar Cells with High Efficiency. *Adv. Energy Mater.* **2020**, *10*, 1902662.
- (33) Lei, T.; Wang, J.-Y.; Pei, J. Design, Synthesis, and Structure-Property Relationships of Isoindigo-Based Conjugated Polymers. *Acc. Chem. Res.* **2014**, *47*, 1117–1126.
- (34) Khan, S.; Lorenzelli, L.; Dahiya, R. S. Technologies for Printing Sensors and Electronics over Large Flexible Substrates: A Review. *IEEE Sens. J.* **2015**, *15*, 3164–3185.
- (35) Enlund, N.; Lovre, M. Advances in Printing and Media Technology; IARIGAI: 2015; Vol. 42.
- (36) Gauthier, C.; Legault, J.; Rondeau, S.; Pichette, A. Synthesis of Betulinic Acid Acyl Glucuronide for Application in Anticancer Prodrug Monotherapy. *Tetrahedron Lett.* **2009**, *50*, 988–991.
- (37) Štella, V. J.; Nti-Addae, K. W. Prodrug Strategies to Overcome Poor Water Solubility. *Adv. Drug Delivery Rev.* **2007**, *59*, 677–694.
- (38) Jain, K.; Kesharwani, P.; Gupta, U.; Jain, N. K. A Review of Glycosylated Carriers for Drug Delivery. *Biomaterials* **2012**, 33, 4166–4186.
- (39) Lei, T.; Guan, M.; Liu, J.; Lin, H.-C.; Pfattner, R.; Shaw, L.; McGuire, A. F.; Huang, T.-C.; Shao, L.; Cheng, K.-T.; Tok, J. B.-H.; Bao, Z. Biocompatible and Totally Disintegrable Semiconducting Polymer for Ultrathin and Ultralightweight Transient Electronics. *Proc. Natl. Acad. Sci. U. S. A.* **2017**, *114*, 5107–5112.
- (40) Lai, K.; Elsas, L. J.; Wierenga, K. J. Galactose Toxicity in Animals. *IUBMB Life* **2009**, *61*, 1063–1074.
- (41) Lei, T.; Dou, J.-H.; Pei, J. Influence of Alkyl Chain Branching Positions on the Hole Mobilities of Polymer Thin-Film Transistors. *Adv. Mater.* **2012**, *24*, 6457–6461.
- (42) Yu, H.; Park, K. H.; Song, I.; Kim, M.-J.; Kim, Y.-H.; Oh, J. H. Effect of the Alkyl Spacer Length on the Electrical Performance of Diketopyrrolopyrrole-Thiophene Vinylene Thiophene Polymer Semiconductors. *J. Mater. Chem. C* **2015**, *3*, 11697–11704.
- (43) Ocheje, M. U.; Charron, B. P.; Cheng, Y.-H.; Chuang, C.-H.; Soldera, A.; Chiu, Y.-C.; Rondeau-Gagné, S. Amide-Containing Alkyl Chains in Conjugated Polymers: Effect on Self-Assembly and Electronic Properties. *Macromolecules* **2018**, *51*, 1336–1344.
- (44) Yao, J.; Yu, C.; Liu, Z.; Luo, H.; Yang, Y.; Zhang, G.; Zhang, D. Significant Improvement of Semiconducting Performance of the Diketopyrrolopyrrole—Quaterthiophene Conjugated Polymer through Side-Chain Engineering via Hydrogen-Bonding. *J. Am. Chem. Soc.* **2016**, *138*, 173–185.
- (45) Guo, L.; Sato, H.; Hashimoto, T.; Ozaki, Y. FTIR Study on Hydrogen-Bonding Interactions in Biodegradable Polymer Blends of Poly(3-Hydroxybutyrate) and Poly(4-Vinylphenol). *Macromolecules* **2010**, 43, 3897–3902.
- (46) Schroeder, B. C.; Kurosawa, T.; Fu, T.; Chiu, Y.-C.; Mun, J.; Wang, G.-J. N.; Gu, X.; Shaw, L.; Kneller, J. W. E.; Kreouzis, T.; Toney, M. F.; Bao, Z. Taming Charge Transport in Semiconducting Polymers with Branched Alkyl Side Chains. *Adv. Funct. Mater.* **2017**, 27, 1701973.

- (47) Selivanova, M.; Chuang, C.-H.; Billet, B.; Malik, A.; Xiang, P.; Landry, E.; Chiu, Y.-C.; Rondeau-Gagné, S. Morphology and Electronic Properties of Semiconducting Polymer and Branched Polyethylene Blends. ACS Appl. Mater. Interfaces 2019, 11, 12723—12732.
- (48) Henderson, R. K.; Jiménez-González, C.; Constable, D. J. C.; Alston, S. R.; Inglis, G. G. A.; Fisher, G.; Sherwood, J.; Binks, S. P.; Curzons, A. D. Expanding GSK's Solvent Selection Guide Embedding Sustainability into Solvent Selection Starting at Medicinal Chemistry. *Green Chem.* **2011**, *13*, 854–862.
- (49) Kipphan, H. Handbook of Print Media: Technologies and Production Methods; Springer-V.; Heidelberg: Berling, 2001.
- (50) Ling, M. M.; Bao, Z. Thin Film Deposition, Patterning, and Printing in Organic Thin Film Transistors. *Chem. Mater.* **2004**, *16*, 4824–4840.
- (51) Teichler, A.; Perelaer, J.; Schubert, U. S. Inkjet Printing of Organic Electronics-Comparison of Deposition Techniques and State-of-the-Art Developments. *J. Mater. Chem. C* **2013**, *I*, 1910–1925.
- (52) Zhang, S.; Ocheje, M. U.; Huang, L.; Galuska, L.; Cao, Z.; Luo, S.; Cheng, Y.-H.; Ehlenberg, D.; Goodman, R. B.; Zhou, D.; Liu, Y.; Chiu, Y.-C.; Azoulay, J. D.; Rondeau-Gagné, S.; Gu, X. The Critical Role of Electron-Donating Thiophene Groups on the Mechanical and Thermal Properties of Donor-Acceptor Semiconducting Polymers. *Adv. Electron. Mater.* **2019**, *5*, 1800899.
- (53) Diao, Y.; Zhou, Y.; Kurosawa, T.; Shaw, L.; Wang, C.; Park, S.; Guo, Y.; Reinspach, J. A.; Gu, K.; Gu, X.; Tee, B. C. K.; Pang, C.; Yan, H.; Zhao, D.; Toney, M. F.; Mannsfeld, S. C. B.; Bao, Z. Flow-Enhanced Solution Printing of All-Polymer Solar Cells. *Nat. Commun.* **2015**, *6*, 1–10.
- (54) Ito, Y.; Virkar, A. A.; Mannsfeld, S.; Oh, J. H.; Toney, M.; Locklin, J.; Bao, Z. Crystalline Ultra Smooth Self-Assembled Monolayers of Alkylsilanes for Organic Field-Effect Transistors. *J. Am. Chem. Soc.* **2009**, 131, 9396–9404.
- (55) Grand, C.; Baek, S.; Lai, T.-H.; Deb, N.; Zajaczkowski, W.; Stalder, R.; Müllen, K.; Pisula, W.; Bucknall, D. G.; So, F.; Reynolds, J. R. Structure-Property Relationships Directing Transport and Charge Separation in Isoindigo Polymers. *Macromolecules* **2016**, *49*, 4008–4022.
- (56) Randell, N. M.; Radford, C. L.; Yang, J.; Quinn, J.; Hou, D.; Li, Y.; Kelly, T. L. Effect of Acceptor Unit Length and Planarity on the Optoelectronic Properties of Isoindigo-Thiophene Donor-Acceptor Polymers. *Chem. Mater.* **2018**, *30*, 4864–4873.
- (Ś7) Zalesskiy, S. S.; Ananikov, V. P. Pd<sub>2</sub>(dba)<sub>3</sub> as a Precursor of Soluble Metal Complexes and Nanoparticles: Determination of Palladium Active Species for Catalysis and Synthesis. *Organometallics* **2012**, *31*, 2302–2309.
- (58) Zhang, S.; Ocheje, M. U.; Luo, S.; Ehlenberg, D.; Appleby, B.; Weller, D.; Zhou, D.; Rondeau-Gagné, S.; Gu, X. Probing the Viscoelastic Property of Pseudo Free-Standing Conjugated Polymeric Thin Films Conjugated Polymeric Thin Films. *Macromol. Rapid Commun.* **2018**, *39*, 1800092–1800100.